Journal Pre-proofs

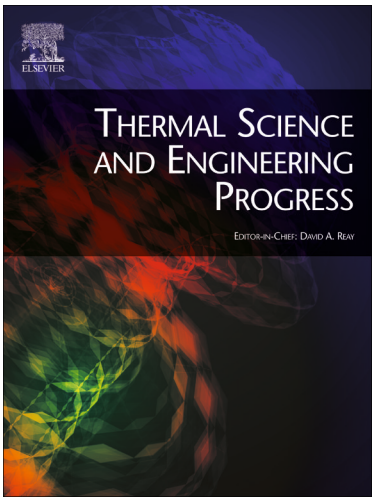

Performance evaluation of helical coils as a passive heat transfer enhancement technique for R134a flow condensation by use of entropy generation analysis

Shahriyar Ghazanfari Holagh, Mohammad Ali Abdous, Mahmood Shafiee, Marc A. Rosen

PII: S2451-9049(21)00076-7
DOI: https://doi.org/10.1016/j.tsep.2021.100914
Reference: TSEP 100914

To appear in: *Thermal Science and Engineering Progress*

Received Date: 6 December 2020
Revised Date: 11 February 2021
Accepted Date: 14 March 2021

Please cite this article as: S.G. Holagh, M.A. Abdous, M. Shafiee, M.A. Rosen, Performance evaluation of helical coils as a passive heat transfer enhancement technique for R134a flow condensation by use of entropy generation analysis, *Thermal Science and Engineering Progress* (2021), doi: https://doi.org/10.1016/j.tsep.2021.100914

Performance evaluation of helical coils as a passive heat transfer enhancement technique for R134a flow condensation by use of entropy generation analysis

Shahriyar Ghazanfari Holagh[a], Mohammad Ali Abdous[a, *1], Mahmood Shafiee[b], Marc A. Rosen[c]

[a]School of Mechanical Engineering, Iran University of Science and Technology, Tehran, Iran

[b]Group of Mechanical Engineering, School of Engineering and Digital Arts, University of Kent, Canterbury, UK

[c]Faculty of Engineering and Applied Science, University of Ontario Institute of Technology, 2000 Simcoe Street North, Oshawa, Ontario, L1G 0C5, Canada

Abstract

Current research focuses on the performance of helically coiled tubes as a passive heat transfer enhancement technique for R134a flow condensation from an entropy generation perspective. Similar to other enhancement techniques, helical coils, are accompanied by pressure drop as a penalty, diminishing their performance, so that these coils are of lower performance compared to straight tubes where the increase in entropy generation due to pressure drop overcomes the decrease in entropy generation due to enhanced heat transfer. Unlike previous studies that have largely investigated heat transfer and pressure drop characteristics of helical coils regardless of their performance, this study employs entropy generation analysis as an effective method to distinguish flow and geometrical conditions at which helical coils are of lower entropy, i.e. higher performance, compared to straight tubes. The findings reveal that, for both helical and straight tubes, entropy generation is enhanced as tube diameter, mass velocity, vapor quality, and wall heat flux increase and saturation temperature decreases. Additionally, applying helical coils within wider ranges of mass velocities can be justified at lower values of tube ($\leq$ 8.3 mm) and coil diameters ($\leq$ 200 mm), saturation temperatures ($\leq$ 40 °C), and vapor quality ($\leq$ 0.6), and at higher values of wall heat flux ($\geq$ 15 kW/m^2). These results substantiate that employing helical coils in lieu of straight tubes is not justifiable always (for all flow and geometrical conditions) although they are of superior heat transfer performance compared to straight tubes.

Keywords: Entropy Generation; R134a Flow Condensation; Helical Coils; Performance Evaluation, Heat Transfer Enhancement

Nomenclature

[1] Corresponding author:
Mohammad Ali Abdous (Email: Abdous@just.ac.ir)

A	Cross-sectional area (m^2)	**Greek symbols**	
L	Length (m)	ρ	Density (kg. m^{-3})
D_i	Tube inner diameter (mm)	v	Specific volume ($m^3.kg^{-1}$)
D_c	Coil inner diameter (mm)	μ	Dynamic viscosity ($Ns.m^{-2}$)
D_r	Diameter ratio		
P	Perimeter (m)	**Subscripts**	
dz	Element discretization (m)	ht	Heat transfer
G	Mass velocity ($kg.m^{-2}.s^{-1}$)	pd	Pressure drop
$\dot{m}$	Mass flow rate ($kg.s^{-1}$)	in	Inlet
T	Temperature (°C)	l	Liquid
x	Vapor quality	sat	Saturation
p	Pressure (Pa)	tp	Two-phase
q	Heat flux ($W.m^{-2}$)	v	Vapor
$\dot{Q}$	Heat rate (W)	w	Wall
U	Convective heat transfer coefficient ($W.m^{-2}.K^{-1}$)		
N_s	Entropy generation number		
h	Specific enthalpy ($J.kg^{-1}$)		
k	Thermal conductivity ($W.m^{-1}K^{-1}$)		
c_p	Heat capacity ($kJ.kg^{-1}K^{-1}$)		
s	Specific entropy ($J.kg^{-1}K^{-1}$)		
$\dot{S}'_{gen}$	Total entropy generation rate per unit length ($W.m^{-1}.K^{-1}$)		
$\dot{S}'_{gen-ht}$	Entropy generation rate per unit length due to heat transfer ($W.m^{-1}.K^{-1}$)		
$\dot{S}'_{gen-pd}$	Entropy generation rate per unit length due to pressure drop ($W.m^{-1}.K^{-1}$)		

1. Introduction

Helical coils are widely used in industrial applications such as heat recovery processes, power generation and thermal processing, refrigeration, steam generation, air conditioning, and food processing. Compared with straight tubes, helical coils are advantageous due to their higher heat transfer coefficient (HTC) and compactness [1]. Nonetheless, phenomena like radial pressure gradient, centrifugal effects, secondary flow, and higher turbulence occurring inside curved tubes [2–4], which improve the HTC, cause pressure drops that diminish the performance of such heat exchangers. Also, one of the main applications of helical coils is in condensers, where the flow experiences a phase change from vapor to liquid together with other complexities, which can further compound the problem.

Numerous researchers have studied heat transfer and pressure drop characteristics of R134a flow condensation inside helical coils. Kang et al. [5] carried out an experimental study on the condensing flow of R134a in a vertical smooth helical coil. They found that an increase in the refrigerant mass velocity leads to enhancements in both overall condensation heat transfer coefficient and pressure drop. R134a flow condensation in horizontal, vertical, and inclined

helical coils was experimentally investigated by Yu et al. [6]. The results indicated that coil orientation significantly affects condensation HTC; that is, in the inclined and vertical positions, it has the highest and lowest values, respectively. Han et al. [7] performed an experimental investigation of heat transfer and pressure drop characteristics of R134a flow condensation in an annular helical tube, and observed that refrigerant mass velocity and saturation temperature considerably influence HTC. The effects of heat flux, mass flux, and condensation temperature on HTC and pressure drop during R134a flow condensation inside a helically coiled tube-in-tube heat exchanger was experimentally studied by Wongwises and Polsongkram [8]. It was deduced that, compared with smooth tubes, the pressure drop of the helically coiled tube is 29-46% higher, while the HTC is 33-53% larger. Lin and Ebadian [9] conducted a series of experiments to evaluate R134a flow condensation inside helical coils with various orientations. It was found that the Nusselt number is larger for lower saturation temperatures and higher refrigerant flow rates. Also, the enhancement in refrigerant Nusselt number is two times greater for inclination angles between 0°-45° than between 45°-90°. Li et al. [10] studied R134a flow condensation inside both straight and helically coiled tube-in-tube heat exchangers and found that the HTC of the helical coil is 4-13.8% higher than that of the straight tube. In addition, the average HTC rises with increasing refrigerant mass velocity and vapor quality.

Many studies have also investigated flow condensation of other refrigerants in helical coils and obtained similar results. Mozafari et al. [11] studied R600a flow condensation inside helical coils with various orientations. The findings demonstrated that maximum values of HTC and pressure drop occur for saturation temperatures more than 30°C and an inclination angle of 0°. Salimpour et al. [12] experimentally investigated R404a flow condensation in a horizontal helical coil. They found that an increase in coil curvature diameter and a decrease in coil pitch lead to substantial enhancements in HTC. An experimental study on R600a flow condensation inside smooth and dimpled helical coils were conducted by Sarmadian et al. [13]. The comparison showed that the HTC of the dimpled tube is 1.2-2 greater than that of the smooth one, whilst its pressure drop is just 58%-195% times higher compared to the smooth one. Solkani and Kumar [14–16] experimentally analyzed heat transfer and pressure drop characteristics of R134a and R600a flow condensation inside smooth, micro-fin, and dimpled helical coils. It was concluded that the HTCs of R-600a flow condensation are roughly 64-128% and 92-132% greater than those of R-134a flow condensation in smooth and dimpled helical coils, respectively. Zakeralhoseini et al.

[17] examined experimentally R1234yf flow condensation in a helical coil and showed that the HTC of the helical coil is 60-120% greater compared with the straight tube with a pressure drop penalty in the range of 46-108%.

As the results of the above-mentioned studies indicate, although the employment of helical coils improves the HTC for flow condensation, it increases pressure drops, diminishing the efficiency of such an enhancement technique. Therefore, entropy generation, as a practical and reliable approach, should be adopted to evaluate heat transfer augmentation along with pressure drop for helical coils to distinguish geometrical and flow conditions for which the thermal and hydraulic losses are of the lowest values. Also, flow and geometrical conditions at which the helical coils achieve higher performance compared to straight tubes and their employment is favorable can be distinguished. Additionally, entropy generation analysis can identify the range at which flow and geometrical parameters can be manipulated to reduce entropy generation and thereby preventing energy loss and improve energy efficiency.

Many researchers have either employed existing or developed new mathematical models to study entropy generation during two-phase flows (both flow boiling and condensation). Collado [18] introduced a one-dimensional model neglecting the pressure drop term to analyze entropy generation of sub-cooled flow boiling. The effects of design parameters on entropy generation during R-134a flow boiling in straight tubes were investigated by Eskin and Deniz [19] utilizing entropy generation analysis. Revellin et al. [20] developed a mathematical model to evaluate local entropy generation during the diabatic saturated two-phase flow of a pure fluid in both plain and enhanced tubes. According to the results, the enhanced tube was favorable at low mass velocities from an entropy generation standpoint. Subsequently, diabatic two-phase flows of R-134a pure refrigerant and a refrigerant-oil mixture were optimized by Revellin and Bonjour [21] utilizing entropy generation analysis as a criterion together with the model developed in the previous study. The authors also found that an increase in oil concentration contributes to higher entropy generation. The models developed by Revellin and colleagues were applied by Abdous et al. [22–24] and Holagh et al. [25] to analyze entropy generation during R-134a flow boiling inside helical coils, micro-fin and twisted-tape tubes as well as plain straight tubes. They distinguished flow and geometrical conditions at which entropy generation is lower in the enhanced tubes compared to the plain ones.

Some studies have assessed entropy generation during condensation. A model was developed by Adeyinka and Naterer [26] to analyze and minimize entropy generation of laminar film condensation on an isothermal plate. The optimization results showed that entropy generation analysis is a useful method to design thermally two-phase flow systems. Li and Yang [27] derived two expressions to compute and minimize entropy generation of free convection film-wise condensation on an elliptical cylinder. They found that local heat transfer coefficient improves with increasing ellipticity, but that the entropy generation increases. The second law of thermodynamics was employed by Dung and Yang [28] to optimize free convection film-wise condensation of saturated vapor on a horizontal tube. The findings revealed that the heat transfer contribution to entropy generation changes as the square of Nusselt number, whereas the gravity-driven film flow friction contribution to entropy generation varies in direct relation with Brinkman number. Saturated vapor film condensation on an isothermal sphere was optimized by Tzeng and Yang [29] adopting the same approach. Regarding the results, it was deduced that as Brinkman and Rayleigh numbers rise, entropy generation increases. The impacts of geometrical parameters and Brinkman and Reynolds numbers on irreversibility during flow condensation on a horizontally positioned isothermal elliptical tube were studied by Esfahani et al. [30]. The ellipticity was found to affect significantly the entropy generation. An entropy generation model was proposed by Ye and Lee [31] to optimally design a refrigerant circuit for a fin-and-tube condenser, and the obtained circuit proved superior in terms of heat transfer performance and entropy generation compared to plain refrigerant circuitries. Sheikholeslami et al. [32] experimentally assessed entropy generation together with exergy loss of nano-refrigerant flow condensation inside a horizontal tube. They investigated the influence of nanoparticle concentration, mass velocity, and vapor quality on entropy generation and found that frictional pressure drop and subsequently entropy generation is enhanced as the concentration of nanoparticles increases. A series of numerical simulations were carried out by Vatanmakan et al. [33] to analyze the influence of volumetric heating on entropy generation for steam condensation in the cascade of turbine blades using the two-phase Eulerian-Eulerian model and the SST k-ω turbulence model. The results revealed that entropy generation declines as volumetric heating increases. Ding et al. [34] simulated the same phenomenon to study the effect of roughness on entropy generation and discovered that entropy generation increases as the blades' roughness increases.

To the best knowledge of the authors, R134a flow condensation inside helical coils has not been analyzed from an entropy generation perspective. In addition, there is no comparative study on R134a flow condensation entropy generation between helical coils and straight tubes by which favorable geometrical and flow conditions for the use of helical coils can be distinguished. Therefore, not only is there no clear comprehension of hydraulic and thermal losses occurring inside helical coils, but also the favorable operating conditions are unknown for such a heat transfer enhancement technique (HTET). Hence, the main objective of the present study is to analyze and compare the entropy generation of R134a flow condensation inside helical coils and straight tubes. To achieve this goal, first, a mathematical model is introduced based on which entropy generation calculation is done under the same flow and geometrical conditions for both tubes, and the impacts of variation in tube diameter in the refrigerant side (D_i), mass velocity (G), vapor quality (x), saturation temperature (T_{sat}), and wall heat flux (q) on entropy generation inside both types of tubes are studied. Then, entropy generation number (N_s) is compared at various geometrical and flow conditions between the helical coil and the straight tube to determine the conditions that are favorable for using the helical coil rather than the straight tube. It is worth noting that the results and the method described in this paper can be utilized by engineers and researchers for designing not only helically-coiled tube-in-tube condensers, but also condensers enhanced by other HTETs like micro-channels, micro-fin tubes, dimple tubes, twisted-tape tubes, and so on in order to minimize the potential thermal losses and pressure drops.

2. Modeling

2.1. Mathematical model

In this section, the mathematical model modified here for analyzing entropy generation of R134a flow condensation inside the helical coil and straight tube is presented. It is noted that the original model upon which this work is based was first proposed by Revellin et al. for saturated two-phase flows [20] and then further developed for refrigerant and refrigerant-oil mixture flow boiling in enhanced tubes[21]. Also, the original model was employed by Abdous et al. [22–24] and Holagh et al. [25] to investigate entropy generation of R134a flow boiling in helical coils, and micro-fin and twisted-tape tubes. In this study, the model is modified to examine entropy

generation of R134a flow condensation inside a helical coil and a straight tube through employing correlations developed by Wongwises et al. [8] and Nualboonrueng et al. [35,36] for predicting Nusselt number and pressure drop.

The entropy generation rate per unit length ($\dot{S}'_{gen}$) for a control volume of length dz can be written based on thermodynamics second law as follows [21]:

$$\dot{S}'_{gen}dz = d[\dot{m}_v s_v + \dot{m}_l s_l] - \delta\dot{Q}/T_w \quad (1a)$$

$$\dot{S}'_{gen}dz = \dot{m}d[x s_v + (1-x)s_l] - \delta\dot{Q}/T_w \quad (1b)$$

$$x = \dot{m}_v/(\dot{m}_v + \dot{m}_l) = \dot{m}_v/\dot{m} \quad (2)$$

where $\dot{m}$, x, s, T_W, and $\delta\dot{Q}$ correspondingly denote mass flow rate, vapor quality, specific entropy, wall temperature, and the differential heat transfer rate to the control volume. Also, subscripts v, l, and w respectively represent vapor, liquid, and wall.

Eq. (1b) can be simplified as follows by noting $s_{lv} = s_v - s_l$:

$$\dot{S}'_{gen}dz = \dot{m}[s_v dx + x ds_v - s_l dx + (1-x)ds_l] - \delta\dot{Q}/T_w \quad (3a)$$

$$\dot{S}'_{gen}dz = \dot{m}[s_{lv} dx + x ds_v + (1-x)ds_l] - \delta\dot{Q}/T_w \quad (3b)$$

The term s_{lv} in Eq. (3b) is defined as follows [22]:

$$s_{lv} = h_{lv}/T_{sat} \quad (4)$$

It is noted that

$$dh_v = T_v ds_v + v_v dp_v \quad (5)$$

$$dh_l = T_l ds_l + v_l dp_l \quad (6)$$

Substituting s_{lv}, ds_v, and ds_l from Eqs. (4)-(6) into Eq. (3b) and assuming $T_{sat} = T_v = T_l$ and $dp = dp_v = dp_l$ for flow condensation, Eq. (3b) can be rewritten as Eq. (7a) or in a more simplified form as Eq. (7b). That is,

$$\dot{S}'_{gen}dz = \dot{m}\left[\frac{h_{lv}}{T_{sat}}dx + x\frac{(dh_v - v_v dp)}{T_{sat}} + (1-x)\frac{(dh_l - v_l dp)}{T_{sat}}\right] - \frac{\delta\dot{Q}}{T_w} \tag{7a}$$

$$\dot{S}'_{gen}dz = \frac{\dot{m}}{T_{sat}}\left[h_{lv}dx + xdh_v + (1-x)dh_l\right] - \frac{\delta\dot{Q}}{T_w} - \frac{\dot{m}\left[xv_v + (1-x)v_l\right]}{T_{sat}}dp \tag{7b}$$

Therefore, $\dot{S}'_{gen}$ can be written in the form of Eq. (8), where dh_{tp} and v_{tp} are obtained using Eqs. (9) and (10), correspondingly [21], as follows:

$$\dot{S}'_{gen}dz = \frac{\dot{m}}{T_{sat}}dh_{tp} - \frac{\delta\dot{Q}}{T_w} - \frac{\dot{m}v_{tp}dp}{T_{sat}} \tag{8}$$

$$dh_{tp} = h_{lv}dx + xdh_v + (1-x)dh_l \tag{9}$$

$$v_{tp} = xv_v + (1-x)v_l \tag{10}$$

Applying the first law of thermodynamics and assuming kinetic energy and gravitational terms to be negligible, $\delta\dot{Q}$ can be attained [21]:

$$d\dot{Q} = \dot{m}dh_{tp} \tag{11}$$

Finally, the entropy generation rate per unit length can be written as follows by substituting Eq. (11) into Eq. (8) and performing further simplifications:

$$\dot{S}'_{gen} = \dot{m}\left[\frac{dh_{tp}}{dz}\left(\frac{1}{T_{sat}} - \frac{1}{T_w}\right) - \frac{v_{tp}\,dp}{T_{sat}dz}\right] \tag{12}$$

Eq. (12) can be divided into two parts:

$$\dot{S}'_{gen-ht} = \dot{m}\left[\frac{dh_{tp}}{dz}\left(\frac{1}{T_{sat}} - \frac{1}{T_w}\right)\right] \quad (13)$$

$$\dot{S}'_{gen-pd} = \frac{\dot{m}v_{tp}}{T_{sat}}\left(-\frac{dp}{dz}\right) \quad (14)$$

The first part, given in Eq. (13), represents the heat transfer contribution to entropy generation, whilst the second part, expressed in Eq. (14), represents the pressure drop contribution to entropy generation.

The term $\frac{dh_{tp}}{dz}$ in Eq. (13) can be replaced with Eq. (15) applying Eq. (16), where q, U, and P signify wall heat flux, heat transfer coefficient, and tube perimeter, correspondingly.

$$q = U(T_w - T_{sat}) = \delta\dot{Q}/Pdz = \dot{m}dh_{tp}/Pdz \quad (15)$$

$$\frac{dh_{tp}}{dz} = \frac{pq}{\dot{m}} \quad (16)$$

Therefore, the simplified form of Eq. (13) can be written in the following form, representing the heat transfer contribution to entropy generation with respect to $T_w - T_{sat} = \frac{q}{U}$:

$$\dot{S}'_{gen-ht} = \frac{q^2P}{UT_wT_{sat}} \quad (17)$$

Here, wall temperature is attained using the wall heat flux and the heat transfer coefficient as known values.

The term $\frac{dp}{dz}$ in Eq. (14), showing the pressure drop contribution to entropy generation, represents the total pressure drop per unit length during flow condensation [8]:

$$\left(\frac{dp}{dz}\right) = \left(\frac{dp_F}{dz}\right)_{tp} + \left(\frac{dp_G}{dz}\right)_{tp} + \left(\frac{dp_A}{dz}\right)_{tp} \quad (18)$$

The terms on the right-hand side of Eq. (18) represent frictional ($\left(\frac{dp_F}{dz}\right)_{tp}$), gravitational ($\left(\frac{dp_G}{dz}\right)_{tp}$), and accelerational ($\left(\frac{dp_A}{dz}\right)_{tp}$) components of the total pressure drop.

The gravitational term is calculated by Eq. (19), where θ and α individually signify the helix angle of the coil and void fraction obtained by Eq. (20) [8]:

$$\left(\frac{dp_G}{dz}\right)_{tp} = [\alpha\rho_v + (1-\alpha)\rho_l]g\sin\theta \tag{19}$$

$$\alpha = \frac{1}{1 + S(\frac{1-x}{x})\frac{\rho_v}{\rho_l}} \tag{20}$$

Here, S denotes the slip ratio, which is expressed by a correlation proposed by Chisholm [37]:

$$S = [1 - x(1 - \frac{\rho_l}{\rho_v})]^{0.5} \tag{21}$$

where ρ_l and ρ_v denote liquid and vapor phase densities of the refrigerant, respectively.

The accelerational term can be written as

$$\left(\frac{dp_A}{dz}\right)_{tp} = G^2\frac{d}{dz}\left[\frac{x^2}{\alpha\rho_v} + \frac{(1-x)^2}{(1-\alpha)\rho_l}\right] \tag{22}$$

where G is the refrigerant mass velocity.

The frictional pressure drop of a gas-liquid two-phase flow can be expressed as [8]

$$\emptyset_l^2 = \left(\frac{dp_F}{dz}\right)_{tp} \Big/ \left(\frac{dp_F}{dz}\right)_l \tag{23}$$

where $\emptyset_l^2$ denotes the two-phase frictional multiplier and $\left(\frac{dp_F}{dz}\right)_l$ the single-phase liquid pressure drop, which can be expressed as [8]

$$\left(\frac{dp_F}{dz}\right)_l = \frac{2f_l\rho_l U_l^2}{D_i} \tag{24}$$

Here, f_l denotes the friction factor, and is defined by Ito [38] for single-phase flow inside a curved tube as follows:

$$f_l\left(\frac{D_c}{D_i}\right)^{0.5} = 0.00725 + 0.076\left[Re_l\left(\frac{D_c}{D_i}\right)^{-2}\right]^{-0.25} \quad (25)$$

The Martinelli parameter X^2 is defined as

$$X^2 = \left(\frac{dp_F}{dz}\right)_l \Big/ \left(\frac{dp_F}{dz}\right)_v \quad (26)$$

If the flow is turbulent, then

$$X = X_{tt} \approx \left(\frac{1-x}{x}\right)^{0.9}\left(\frac{\rho_v}{\rho_l}\right)^{0.5}\left(\frac{\mu_l}{\mu_v}\right)^{0.1} \quad (27)$$

The two-phase frictional multiplier can be expressed for a smooth circular tube with the Lockhart-Martinelli correlation:

$$\emptyset_l^2 = 1 + \frac{C}{X_{tt}} + \frac{1}{X_{tt}^2} \quad (28)$$

where C is a parameter showing the two-phase flow condition and its value for different flow conditions is variable (between 5 and 20) [38]. Substitution of Eqs. (24) and (28) into Eq. (23) results in an expression for the frictional two-phase pressure drop.

In order to apply this model to analyze entropy generation of R-134a flow condensation in a helical coil and a straight tube, four experimental correlations are required. Two correlations, one for the helical coil and another for the straight tube, should be employed for Nusselt number that is used in the determination of HTC (Eq. (17)). Also, two correlations for $\emptyset_l^2$ that is used in the calculation of frictional pressure drop (Eq. (23)) for these tubes. As previously mentioned, heat transfer and pressure drop characteristics of R-134a flow condensation in a helically-coiled tube-in-tube heat exchanger were experimentally studied by Wongwises et al. [8]. In accordance with this study, two-phase Nusselt number, $Nu_{tp,}$ (Eq. (29)) can be expressed in terms of Martinelli

parameter (X_{tt}), equivalent Dean number (De_{Eq}), Prandtl number (Pr_l), reduced pressure (p_r), and Boiling number (Bo), which can be correspondingly computed using Eqs. (27) and (29)-(33), as follows:

$$Nu_{tp-\text{helical coil}} = 0.1352 De_{Eq}^{\ 0.7654} Pr_l^{0.8144} X_{tt}^{\ 0.0432} p_r^{\ -0.3256} (Bo \times 10^4)^{0.112} \quad (29)$$

$$De_{Eq} = \left[Re_l + Re_v \left(\frac{\mu_v}{\mu_l}\right)\left(\frac{\rho_l}{\rho_v}\right)^{0.5} \right]\left(\frac{D_i}{D_c}\right)^{0.5} \quad (30)$$

$$Pr_l = \frac{Cp_l \mu_l}{k_l} \quad (31)$$

$$p_r = \frac{P_{sat}}{P_{crit}} \quad (32)$$

$$Bo = \frac{q''}{G h_{lv}} \quad (33)$$

Here, Re_l and Re_v respectively denote liquid and vapor Reynolds numbers, which can be written as

$$Re_l = \frac{G(1-x)D_i}{\mu_l} \quad (34)$$

$$Re_v = \frac{GxD_i}{\mu_v} \quad (35)$$

As for two-phase frictional multiplier ($\emptyset_l^2$), Wongwises et al. [8] propose the following:

$$\emptyset_{l-\text{helical coil}}^2 = 1 + \frac{5.569}{X_{tt}^{\ 1.496}} + \frac{1}{X_{tt}^{\ 2}} \quad (36)$$

In addition to these correlations, the correlations developed by Nualboonrueng et al. [35,36] are utilized to calculate HTC (Eq. (37)) and pressure drop (Eq. (39)), and subsequently entropy generation of R134a flow condensation inside the straight tube, as follows:

$$Nu_{tp-\text{straight tube}} = 0.003 Re_{Eq}^{\ 0.997} Pr_l^{0.932} \quad (37)$$

$$Re_{Eq} = Re_l + Re_v \left(\frac{\mu_v}{\mu_l}\right)\left(\frac{\rho_l}{\rho_v}\right)^{0.5} \quad (38)$$

$$\emptyset_{l-\text{straight tube}}^2 = 1 + \frac{5.705}{X_{tt}^{1.711}} \quad (39)$$

As the above-mentioned correlations have been developed to determine the HTC and the pressure drop of R134a flow condensation inside helical coils and straight tubes and are in good agreement with not only experimental results obtained by Wongwises et al. [8] and Nualboonrueng et al. [35,36], but also findings of other researchers [11,14–17,39,40] for various flow and geometrical conditions, they are suitable for use in the aforementioned model.

The entropy generation number, defined as the ratio of entropy generation rate in the helical coil ($\dot{S}'_{gen-hc}$) to entropy generation rate in the plain straight tube ($\dot{S}'_{gen-st}$), is defined as

$$N_s = \dot{S}'_{gen-hc}/\dot{S}'_{gen-st} \quad (40)$$

Note that the effectiveness of the helical coil relative to the plain straight tube can be determined utilizing N_s. In essence, a value of $N_s < 1$ indicates that the helical coil exhibits superior performance with respect to the plain straight tube, and vice versa.

It is also noted that, in the developed numerical code, R-134a thermo-physical properties are calculated employing the following polynomial functions for each element [25]:

$$\text{property} = a_0 + a_1T + a_2T^2 + a_3T^3 + a_4T^4 + a_5T^5 \quad (41)$$

$$\ln(\text{property}) = a_0 + a_1T + a_2T^2 + a_3T^3 + a_4T^4 + a_5T^5 \quad (42)$$

Coefficients a_0 to a_5 are provided in Table 1. Eq. (41) is applied to obtain the values of p_v, ρ_v and k_v, whereas Eq. (42) is employed to compute values of h_{lv}, ρ_l, μ_v, μ_l, k_l, σ, c_{pl} and c_{pv}.

2.2. Physical model

The schematic of a helical coil and important dimensions embracing refrigerant side tube diameter (D_i), and coil diameter are illustrated in Fig. 1. The helical coil and the plain straight tube are divided into 4000 one-dimensional control volume elements (cells), satisfying grid independency as demonstrated in Figs. 3a and 3b. Saturated R-134a flows through the inner tube, while cold water passes through the annular part in both the helical coil and plain straight tube. It is worth noting that the tubes are made of copper. For simulations, the considered coil pitch is 35

mm and the number of turns of the helical coil is 2.6. Both helical coil and straight tube are 2500 mm in length in order to have a reliable comparison on entropy generation between the tubes.

2.3. Method of solution

To conduct the entropy generation analysis, a numerical code was developed in MATLAB based on the model described above. To have a clear understanding of conducted simulations, the method of solution is expounded. First, the considered geometries are divided into a number of cells that must fulfill a grid independency requirement. Then, mass, momentum, and energy equations are coupled for each cell in a loop to attain the local wall temperature, local liquid temperature, and local pressure. Once these parameters are calculated, the fluid thermo-physical properties are computed and used to find the amount of the generated entropy and relevant parameters in each cell utilizing the entropy generation model. During these calculations, the correlations proposed by Wongwises et al. [8] and Nualboonrueng et al. [35,36] for the pressure drop and heat transfer coefficient are employed. In order to verify the accuracy of the results obtained for entropy generation, total entropy generation is calculated by integrating over the whole geometry and then compared with the R-134a entropy values reported in the thermodynamic charts. If the results show that the difference between the total entropy generation attained from the calculations and that obtained from the thermodynamic charts is less than 10^{-5}, the calculation results are considered sufficiently accurate, ending the calculations. Note that because of the complex nature of two-phase flows and the associated heat transfer, relevant parameters like void fraction and quality are appropriately determined.

2.4. Validation

The grids considered for both helical coil and straight tube are one-dimensional. Since the simulations are thermodynamic-based intending to calculate the amount of generated entropy inside the tubes, the application of one-dimensional grids is appropriate and justifiable. Figs. 2a and 2b reveal the zoomed views of the devised grids for the helical coil and straight tube, respectively. In fact, both girds consist of 4000 cells distributed along a helical curve and a straight line passing through the center of the helical coil and straight tube, respectively, and are placed in 0.625 mm distances.

Validation and grid independency evaluations of the model and method of solution for the helical coil and straight tube are plotted in Figs. 3a and 3b, respectively. For both tubes, the validation was conducted at three different values of mass flux (240, 520, and 720 kg/m^{2}s) and saturation temperature, inlet quality, and wall heat flux of 40 °C, 0.8, and 5000 W/m^2, respectively. As can be seen, the value of entropy generation reaches a fixed value equal to that obtained from thermodynamics charts after the point corresponding to 4000 cells. This suggests that 4000 cells are sufficient for the considered geometry.

3. Results and discussion

The results attained from entropy generation analysis are now considered. First, the impacts of flow and geometrical parameters on entropy generation and heat transfer and pressure drop contributions to entropy generation inside both types of tubes are provided. Then, regarding entropy generation number, geometrical and flow conditions at which the helical coil exhibits superior performance are identified. It is noted that the flow conditions reported in Table 2 together with tube and coil diameters of 8.3 mm and 305 mm, respectively, and coil pitch of 35 mm are used as input data; otherwise, conditions are as stated. These parameters are selected as input parameters since they are within the ranges of the parameters studied by Wongwises et al. [8] and Nualboonrueng et al. [35,36] whose suggested correlations for HTC and pressure drop have been employed in the present mathematical model.

3.1. Influence of geometrical and flow parameters

3.1.1. Influence of tube diameter

The variations of entropy generation and its components with tube diameter are demonstrated in Fig. 4 for both the helical coil and the straight tube. For both the tubes, heat transfer and pressure drop contributions to entropy generation and total entropy generation are seen to rise as tube diameter increases from 5 to 25 mm. An increase in the tube diameter results in a larger tube cross-sectional area and, therefore, the mass flow rate of R134a flow entering the tubes rises at constant mass velocity. Consequently, the difference between the saturation and wall temperatures becomes larger, leading to an enhancement in the heat transfer contribution to entropy generation**.** Also, since the HTC of the helical coil is greater than that of the straight

tube, the heat transfer contribution to entropy generation of the helical coil is lower compared with the straight tube. However, when the wall heat flux is constant, the mass flow rate is proportional to the second power of the tube diameter, but the heat transfer from the wall to flow is proportional to the tube diameter. That is, as the tube diameter increases, the effect of the increase in mass flow rate on two-phase mixture density overcomes the effect of heat transfer, resulting in a reduction in two-phase mixture density. As a result, the two-phase mixture flow velocity increases at constant mass velocity, thereby increasing the pressure drop inside the tubes and its contribution to entropy generation. Note that, as the pressure drop is greater than in the helical coil than the straight tube, the pressure drop contribution to entropy generation inside the coil is found to be higher as shown in Fig. 4. Eventually, the total entropy generation of the helical coil exceeds that of the straight tube since the pressure drop contribution to entropy generation is larger than the heat transfer contribution.

3.1.2. Influence of mass velocity

The influence of mass velocity on entropy generation and its components for the helical coil and straight tube is shown in Fig. 5. It is seen for both tubes that, as mass velocity increases from 200 to 600 kg/m^{2}s, the pressure drop contribution to entropy generation rises while heat transfer contribution declines. In essence, the flow velocity inside the tubes increases with the mass velocity, contributing to a rise in both HTC due to higher turbulence and pressure drop due to higher frictional loss. Therefore, the heat transfer contribution declines while the pressure drop contribution increases. Due to the higher pressure drop and HTC inside the helical coil, this tube exhibits a higher pressure drop contribution and lower heat transfer contribution compared to the straight tube. It is also seen that as mass velocity increases, the difference between the pressure drop contributions of the tubes becomes larger, while the difference between the heat transfer contributions becomes smaller so that, at mass velocities higher than 500 kg/m^{2}s, both tubes have nearly the same amount of heat transfer contribution.

A careful inspection of Fig. 5 reveals that, for mass velocities less than 340 kg/m^{2}s, the total entropy generation of the straight tube is greater than that of the helical coil. This is due to the fact that the heat transfer contribution of the straight channel exceeds that of the helical coil since both the tubes have nearly the same values of pressure drop contribution at mass velocities lower than 340 kg/m^{2}s. At mass velocities higher than 340 kg/m^{2}s, the heat transfer contribution of the straight tube nears that of the helical coil, while the difference between the pressure drop

contributions of the tubes becomes larger. Thus, the total entropy generation of the helical coil outweighs the total entropy generation of the straight tube above a mass velocity of 340 kg/m^{2}s.

3.1.3. Influence of saturation temperature

The variations in entropy generation and its components against saturation temperature are illustrated in Fig. 6. As the saturation temperature rises from 30 ℃ to 50 ℃, it is observed that the pressure drop contributions and the total entropy generations of both the tubes decline, whilst the heat transfer contributions grow. In essence, higher saturation temperatures imply higher saturation pressures. However, at a constant mass flux, the higher the saturation pressure is, the higher is the mixture density, leading to lower flow velocities and subsequently lower pressure drops. Thus, pressure drop contribution to entropy generation of both the tubes decreases. Since the helical coil experiences a higher pressure drop compared with the straight tube, its pressure drop contribution to entropy generation is greater. In addition, the decline in flow velocity causes reductions in the HTC of both tubes, contributing to further entropy generation due to heat transfer, as demonstrated in Fig. 6. Note that, since the HTC of the helical coil is higher than that of the straight tube, its heat transfer contribution to entropy generation is lower.

3.1.4. Influence of vapor quality

Fig. 7 shows the impact of varying vapor quality on entropy generation and its components for both tubes. It is seen that the total entropy generations and their pressure drop components experience increasing trends, whereas the heat transfer contributions exhibit decreasing trends as the vapor quality increases from 0.4 to 0.9. These trends occur because, as the mass velocity remains unchanged, an increase in vapor quality results in a reduction in the two-phase mixture density and, consequently, an enhancement in flow velocity. But higher flow velocities inside the tubes lead to higher HTCs and pressure drops and, hence, declining heat transfer contributions and increasing pressure drop contributions to entropy generation. Due to the higher HTC and pressure drop inside the helical coil compared to the straight tube, its heat transfer contribution is lower and its pressure drop contribution greater.

Further inspection of Fig. 7 reveals that for vapor qualities below 0.61, the total entropy generation of the straight tube is higher than that of the helical coil due to its higher heat transfer contribution, while for vapor qualities greater than 0.61, the helical coil exhibits a higher total entropy generation since its pressure drop contribution grows and the straight tube heat transfer contribution becomes closer to that of the helical coil.

3.1.5. Influence of heat flux

The behaviors of the entropy generation and its components as heat flux varies are illustrated in Fig. 8 for both the tubes. It is observed that, with increasing wall heat flux from 5000 to 10000 W/m^2, the heat transfer contributions increase considerably, whereas the pressure drop contributions and the total entropy generations decline slightly. In fact, the condensation process is intensified as the wall heat flux rises, contributing to an enhancement in mass transfer rate. Therefore, the two-phase mixture density increases, leading to a reduction in flow velocity as the mass velocity is kept constant. The decrease in the flow velocity brings about lower HTCs and pressure drops inside the tubes and, thus, increasing heat transfer contributions and decreasing pressure drop contributions to entropy generation. Again, since the HTC pressure drop inside the helical coil is greater than that of the straight tube, its heat transfer and pressure drop contributions are lower and higher respectively compared to the straight tube.

3.2. Favorable geometry and flow conditions

In this subsection, favorable geometrical and flow conditions for R134a flow condensation are examined for which helical coils demonstrate superior performance compared to straight tubes. A value of $N_s < 1$ means that the helical coil exhibits better performance than the straight tube from an entropy generation point of view, and vice versa.

3.2.1. Tube diameter

The variation of N_s with mass velocity is shown in Fig. 9 for two tube diameters. As can be seen, when mass velocity is 340 kg/m^2s, the entropy generation number of the helical coil with the tube diameter of 8.3 mm is $N_s = 1$. This is because the total entropy generation of this helical coil is equal to that of the straight tube at a mass velocity of 340 kg/m^2s (See Fig. 5). At mass velocities lower than 340 kg/m^2s, therefore, the helical coil performs better than the straight tube from an entropy generation standpoint, while at mass velocities higher than 340 kg/m^2s, the straight tube exhibits better performance. Also, it is observed that, compared to the helical coil having a tube diameter of 8.3 mm, the value of N_s crosses the line $N_s = 1$ for the helical coil with tube diameter equal to 20 mm at a lower mass velocity (320 kg/m^2s). That is, as the tube diameter decreases, the use of a helical coil rather than straight tubes becomes justifiable at higher mass velocities.

3.2.2. Coil diameter

Fig. 10 illustrates the variation of N_s with mass velocity for two coil diameters. Similar to Fig. 5, the entropy generation number of the coil with a diameter of 305 mm crosses the line $N_s = 1$ at a mass velocity of 340 kg/m^{2}s, whereas for the coil with lower coil diameter ($D_c = 200$ mm), the N_s curve crosses the line $N_s = 1$ at a higher mass velocity (380 kg/m^{2}s). This means that, as the coil diameter declines, the employment of a helical coil instead of straight tubes can be justifiable at wider ranges of mass velocity.

3.2.3. Saturation temperature

The variation in N_s with mass velocity is shown in Fig. 11 for two values of saturation temperature. According to this figure, the lower is the saturation temperature, the higher is the mass velocity at which the entropy generation number crosses the line $N_s = 1$. For instance, at a saturation temperature of 60 ℃, the N_s value equals one at a mass velocity of 320 kg/m^{2}s, but when the saturation temperature declines to 40 ℃, the mass velocity at which the N_s curve reaches the line $N_s = 1$ rises by 20 kg/m^{2}s. Therefore, the justifiability of applying helical coils within wider ranges of mass velocities can be achieved at lower values of saturation temperature.

3.2.4. Vapor quality

The variation of entropy generation number with mass velocity for two values of vapor quality is plotted in Fig. 12. It is observed that, for a reduction in vapor quality from 0.8 to 0.6, the mass velocity at which the N_s curve crosses the line $N_s = 1$ increases from 340 kg/m^{2}s to 404 kg/m^{2}s. In other words, the mass velocity range, at which the utilization of helical coils rather than straight tubes results in better performance, is widened by 64 kg/m^{2}s when the vapor quality reduces by 0.2.

3.2.5. Heat flux

Fig. 13 presents the variation of N_s with mass velocity for two values of wall heat flux. It is evident that a 5000 W/m^2 enhancement in the wall heat flux (from 10,000 W/m^2 to 15,000 W/m^2) widens the range of the mass velocity at which superior performance is achieved if the helical coil is employed instead of a straight tube, by nearly 90 kg/m^{2}s (from 340 kg/m^{2}s to 430 kg/m^{2}s). That is, the higher the wall heat flux, the wider is the mass velocity at which the entropy generation number is lower than one.

4. Conclusions

R134a flow condensation inside helical coils and straight tubes was analyzed and compared from an entropy generation perspective using a computational code developed in MATLAB. As opposed to the previous studies that mainly focuses on heat transfer and pressure drop characteristics of helical coils, this study used entropy generation analysis to determine the effect of geometrical and flow conditions on entropy generation and distinguish conditions at which the application of helical coils rather than straight tubes for R134a flow condensation results in superior performance. The main outcomes of this study are as follow:

- For the ranges of considered flow and geometrical conditions, the helical coil generally exhibits a higher pressure drop contribution and lower heat transfer contribution to entropy generation compared to straight tubes.
- At constant flow conditions, for both the helical coil and straight tube, the total entropy generation and its pressure drop and heat transfer contributions rise as the tube diameter increases.
- At constant geometrical conditions, total entropy generation increases with increasing mass and wall heat fluxes and vapor quality and decreasing saturation temperature, for both tube types.
- The application of helical coils rather than straight tubes can be justifiable and is of superior performance within a wider range of mass velocity values when the tube and coil diameters, saturation temperature, and vapor quality are of lower values and the wall heat flux is of a higher value.

References

[1] R. Kharat, N. Bhardwaj, R.S. Jha, Development of heat transfer coefficient correlation for concentric helical coil heat exchanger, Int. J. Therm. Sci. 48 (2009) 2300–2308. doi:10.1016/j.ijthermalsci.2009.04.008.

[2] S.G. Holagh, M.A. Abdous, P. Roy, M. Shamsaiee, M. Shafiee, H. Saffari, L. Vali, R. Andersson, An experimental investigation on bubbles departure characteristics during sub-cooled flow boiling in a vertical U-shaped channel utilizing high-speed photography, Therm. Sci. Eng. Prog. 22 (2021). doi:10.1016/j.tsep.2020.100828.

[3] S.G. Holagh, M.A. Abdous, M. Shamsaiee, H. Sa, An experimental study on the influence of radial pressure gradient on bubbles dynamic behavior in subcooled flow boiling, Therm. Sci. Eng. Prog. 16 (2020). doi:10.1016/j.tsep.2019.100468.

[4] M.A. Abdous, S.G. Holagh, M. Shamsaiee, H. Saffari, The prediction of bubble departure and lift-off radii in vertical U-shaped channel under subcooled flow boiling based on forces balance analysis, Int. J. Therm. Sci. 142 (2019) 316–331. doi:10.1016/j.ijthermalsci.2019.04.021.

[5] H.J. Kang, C.X. Lin, M.A. Ebadian, Condensation of R134a flowing inside helicoidal pipe, Int. J. Heat Mass Transf. 43 (2000) 2553–2564. doi:https://doi.org/10.1016/S0017-9310(99)00296-3.

[6] A. Yu, B Han, J.R Kang, H.J Lin, C.X Awwad, M.. Ebadian, Condensation heat transfer of R-134A flow inside helical pipes at different orientations, Int. Commun. Heat Mass Transf. 30 (2003) 745–754. doi:https://doi.org/10.1016/S0735-1933(03)00122-2.

[7] J.T. Han, C.X. Lin, M.A. Ebadian, Condensation heat transfer and pressure drop characteristics of R-134a in an annular helical pipe, Int. Commun. Heat Mass Transf. 32 (2005) 1307–1316. doi:10.1016/j.icheatmasstransfer.2005.07.009.

[8] S. Wongwises, M. Polsongkram, Condensation heat transfer and pressure drop of HFC-134a in a helically coiled concentric tube-in-tube heat exchanger, Int. J. Heat Mass Transf. 49 (2006) 4386–4398. doi:10.1016/j.ijheatmasstransfer.2006.05.010.

[9] C.X. Lin, M.A. Ebadian, Condensation heat transfer and pressure drop of R134a in annular helicoidal pipe at different orientations, Int. J. Heat Mass Transf. 50 (2007) 4256–4264. doi:10.1016/j.ijheatmasstransfer.2007.02.022.

[10] S. Li, J. Han, Su-Guo-ping, J. Pan, Condensation heat transfer of R-134A in horizontal straight and helically coiled tube-in-tube heat exchangers, J. Hydrodyn. Ser. B. 19 (2007) 677–682. doi:https://doi.org/10.1016/S1001-6058(08)60003-7.

[11] M. Mozafari, M.A. Akhavan-Behabadi, H. Qobadi, M. Fakoor, Condensation and pressure drop characteristics of R600a in a helical tube-in-tube heat exchanger at different inclination angles, Appl. Therm. Eng. 90 (2015) 571–578. doi:10.1016/j.applthermaleng.2015.07.044.

[12] M.R. Salimpour, A. Shahmoradi, D. Khoeini, Experimental study of condensation heat transfer of R-404a in helically coiled tubes, Int. J. Refrig. 74 (2016) 584–591. doi:10.1016/j.ijrefrig.2016.12.002.

[13] A. Sarmadian, M. Shafaee, H. Mashouf, S.G. Mohseni, Condensation heat transfer and pressure drop characteristics of R-600a in horizontal smooth and helically dimpled tubes, Exp. Therm. Fluid Sci. 86 (2017) 54–62. doi:10.1016/j.expthermflusci.2017.04.001.

[14] A. Kumar, R. Kumar, Two-phase flow condensation heat transfer characteristic of R-600a inside the horizontal smooth and dimpled helical coiled tube in shell type heat exchanger, Int. J. Refrig. 107 (2019) 155–164. doi:10.1016/j.ijrefrig.2019.07.017.

[15] A.K. Solanki, R. Kumar, Condensation of R-134a inside dimpled helically coiled tube-in-shell type heat exchanger, Appl. Therm. Eng. 129 (2018) 535–548. doi:10.1016/j.applthermaleng.2017.10.026.

[16] A.K. Solanki, R. Kumar, Condensation of R-134a inside micro-fin helical coiled tube-in-shell type heat exchanger, Exp. Therm. Fluid Sci. 93 (2018) 344–355. doi:https://doi.org/10.1016/j.expthermflusci.2018.01.021.

[17] S. Zakeralhoseini, B. Sajadi, M. Ali, A. Behabadi, S. Azarhazin, Experimental investigation of the heat transfer coefficient and pressure drop of R1234yf during flow condensation in helically coiled tubes, Int. J. Therm. Sci. 157 (2020) 106516. doi:10.1016/j.ijthermalsci.2020.106516.

[18] F.J. Collado, The entropy balance for boiling flow, Fusion Eng. Des. 56–57 (2001) 199–203. doi:10.1016/S0920-3796(01)00259-9.

[19] N. Eskin, E. Deniz, Influence of design parameters on two-phase pressure drop and entropy generation during evaporation of refrigerants, in: 22nd Int. Conf. Effic. Cost, Optim. Simul. Environ. Impact Energy Syst., 2009: pp. 159–168.

[20] R. Revellin, S. Lips, S. Khandekar, J. Bonjour, Local entropy generation for saturated two-phase flow, Energy. 34 (2009) 1113–1121. doi:10.1016/j.energy.2009.03.014.

[21] R. Revellin, J. Bonjour, Entropy generation during flow boiling of pure refrigerant and refrigerant-oil mixture, Int. J. Refrig. 34 (2011) 1040–1047. doi:10.1016/j.ijrefrig.2011.01.010.

[22] M.A. Abdous, H. Saffari, H.B. Avval, M. Khoshzat, Investigation of entropy generation in a helically coiled tube in flow boiling condition under a constant heat flux, Int. J. Refrig. 60 (2015) 217–233. doi:10.1016/j.ijrefrig.2015.07.026.

[23] M.A. Abdous, S.G. Holagh, M. Shamsaiee, An evaluation of heat transfer enhancement technique in flow boiling conditions based on entropy generation analysis : micro-fin tube, in: 4th Int. Electron. Conf. Entropy Its Appl., 2017: pp. 1–9. doi:10.3390/ecea-4-05002.

[24] M.A. Abdous, H. Saffari, H. Barzegar Avval, M. Khoshzat, The study of entropy generation during flow boiling in a micro-fin tube, Int. J. Refrig. 68 (2016) 76–93. doi:10.1016/j.ijrefrig.2016.04.008.

[25] S.G. Holagh, M.A. Abdous, M. Shamsaiee, H. Saffari, Assessment of heat transfer enhancement technique in flow boiling conditions based on entropy generation analysis : twisted-tape tube, Heat Mass Transf. 56 (2020) 429–443. doi:https://doi.org/10.1007/s00231-019-02705-y.

[26] O. Adeyinka, G. Naterer, Optimization correlation for entropy production and energy availability in film condensation, Int. Commun. Heat Mass Transf. 31 (2004) 513–524. doi:https://doi.org/10.1016/S0735-1933(04)00032-6.

[27] G. Li, S. Yang, Entropy generation minimization of free convection film condensation on an elliptical cylinder, Int. J. Therm. Sci. 46 (2007) 407–412. doi:10.1016/j.ijthermalsci.2006.06.007.

[28] S. Dung, S. Yang, Second law based optimization of free convection film-wise condensation on a horizontal tube, Int. Commun. Heat Mass Transf. 33 (2006) 636–644. doi:10.1016/j.icheatmasstransfer.2006.01.013.

[29] S.-H. Tzeng, S.-A. Yang, Second law analysis and optimization for film-wise condensation from downward flowing vapors onto a sphere, Heat Mass Transf. 43 (2007) 365–369. doi:10.1007/s00231-006-0119-5.

[30] J.A. Esfahani, M. Modirkhazeni, Entropy generation of forced convection film condensation on a horizontal elliptical tube, Comptes Rendus Mec. 340 (2012) 543–551. doi:10.1016/j.crme.2012.03.008.

[31] H. Ye, K. Lee, Refrigerant circuitry design of fin-and-tube condenser based on entropy generation minimization, Int. J. Refrig. 35 (2012) 1430–1438. doi:10.1016/j.ijrefrig.2012.03.013.

[32] M. Sheikholeslami, M. Darzi, Z. Li, Experimental investigation for entropy generation and exergy loss of nano-refrigerant condensation process, Int. J. Heat Mass Transf. 125 (2018) 1087–1095. doi:10.1016/j.ijheatmasstransfer.2018.04.155.

[33] M. Vatanmakan, E. Lakzian, M. Reza, Investigating the entropy generation in condensing steam fl ow in turbine blades with volumetric heating, Energy. 147 (2018) 701–714. doi:10.1016/j.energy.2018.01.097.

[34] H. Ding, Y. Li, E. Lakzian, C. Wen, C. Wang, Entropy generation and exergy destruction in condensing steam flow through turbine blade with surface roughness, Energy Convers. Manag. 196 (2019) 1089–1104. doi:10.1016/j.enconman.2019.06.066.

[35] T. Nualboonrueng, S. Wongwises, Two-phase flow pressure drop of HFC-134a during condensation in smooth and micro-fin tubes at high mass flux, Int. J. Heat Mass Transf. 31 (2004) 991–1004. doi:https://doi.org/10.1016/j.icheatmasstransfer.2004.05.009.

[36] T. Naulboonrueng, J. Kaewon, S. Wongwises, Two-phase condensation heat transfer coefficients of HFC –134a at high mass flux in smooth and micro-fin tubes, Int. J. Heat Mass Transf. 30 (2003) 577–590. doi:https://doi.org/10.1016/S0735-1933(03)00086-1.

[37] D. Chisholm, Pressure gradients due to friction during the flow of evaporating two-phase mixtures in smooth tubes and channels, Int. J. Heat Mass Transf. 16 (1973) 347–358. doi:https://doi.org/10.1016/0017-9310(73)90063-X.

[38] H. Ito, Friction factors for turbulent flow in curved pipes, J. Basic Eng. 81 (1959) 123–132. doi:https://doi.org/10.1115/1.4008390.

[39] A. Gupta, R. Kumar, A. Gupta, Condensation of R-134a inside a helically coiled tube-in-shell heat exchanger, Exp. Therm. Fluid Sci. 54 (2014) 279–289. doi:10.1016/j.expthermflusci.2014.01.003.

[40] M.E. Mosaad, M. Al-Hajeri, R. Al-Ajmi, A.M. Koliub, Heat transfer and pressure drop of R-134a condensation in a coiled double tube, Heat Mass Transf. 45 (2009) 1107–1115. doi:10.1007/s00231-009-0484-y.

Table 1. Constants for Eqs. (41) and (42)

Property	a_0	a_1	a_2	a_3	a_4	a_5	Error (%)
p_v (10^5 Pa)	2.9283	0.10610	1.476×10^{-3}	9.127×10^{-6}	1.886×10^{-8}	-1.002×10^{-11}	0.03
h_{lv} (kJ/kg)	5.2912	-0.0038266	-1.918×10^{-5}	-1.366×10^{-7}	-1.419×10^{-9}	-1.186×10^{-11}	0.01
ρ_l (10^3 kg/m³)	0.25819	-0.0025548	-8.450×10^{-6}	-5.340×10^{-8}	-6.130×10^{-10}	-4.306×10^{-12}	0.01
ρ_v (kg/m³)	14.323	0.49951	7.608×10^{-3}	6.524×10^{-5}	-4.161×10^{-8}	-4.912×10^{-9}	0.56
μ_l (10^{-3} Ns/m²)	-1.3047	-0.012721	1.307×10^{-5}	-3.630×10^{-7}	6.416×10^{-10}	4.390×10^{-12}	0.05
μ_v (10^{-7} Ns/m²)	4.6756	0.0038342	-2.626×10^{-6}	8.789×10^{-8}	5.076×10^{-10}	6.183×10^{-12}	0.00
k_l (W/m-K)	-2.3865	-0.0047587	-4.998×10^{-6}	-1.537×10^{-7}	-7.550×10^{-10}	2.111×10^{-11}	0.02
k_v (W/m-K)	0.011516	0.00008689	1.232×10^{-7}	2.031×10^{-9}	3.669×10^{-11}	2.864×10^{-13}	0.02
σ (10^{-3} N/m)	2.4473	-0.012448	-5.950×10^{-5}	-4.064×10^{-7}	-4.528×10^{-9}	-3.336×10^{-11}	0.01
$c_{p,l}$ (kJ/kg-K)	0.29357	0.0020423	1.143×10^{-5}	7.946×10^{-8}	1.491×10^{-9}	1.678×10^{-11}	0.01
$c_{p,v}$ (kJ/kg-K)	-0.10828	0.0050590	1.604×10^{-5}	1.136×10^{-7}	2.312×10^{-9}	2.517×10^{-11}	0.02

Table 2. Flow conditions utilized in simulations (Section 3.1)

x	T_{sat} (°C)	G (kg/m²s)	q (W/m²)
0.8	40	400	5000

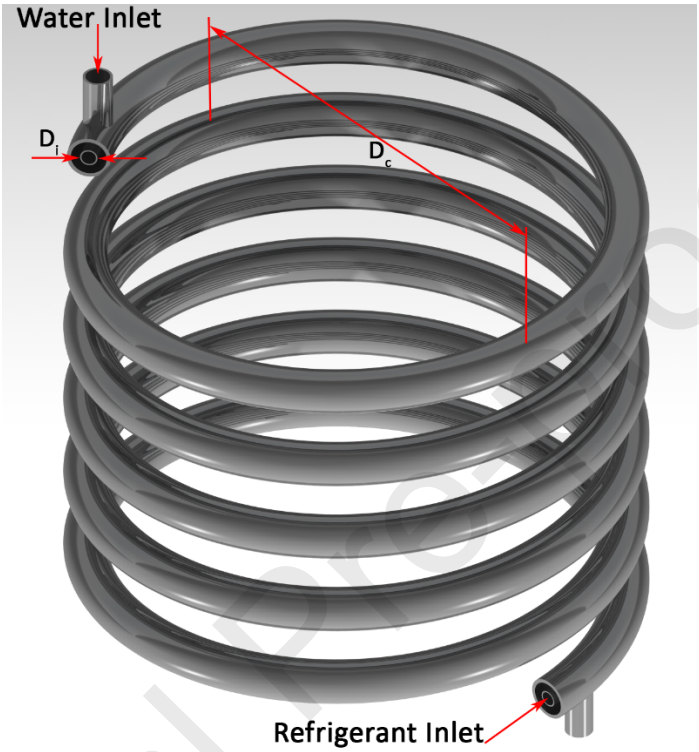

Fig. 1: Schematic of helically coiled tube-in-tube condenser with important geometrical parameters, adopted from Wongwises et al. [8].

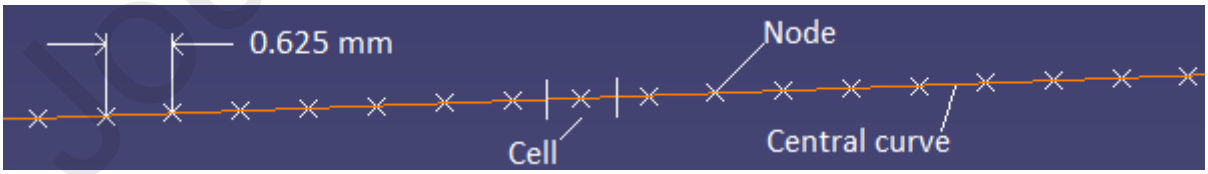

Fig. 2a: Zoomed view of the grid considered for the helical coil

Fig. 2b: Zoomed view of the grid considered for the straight tube

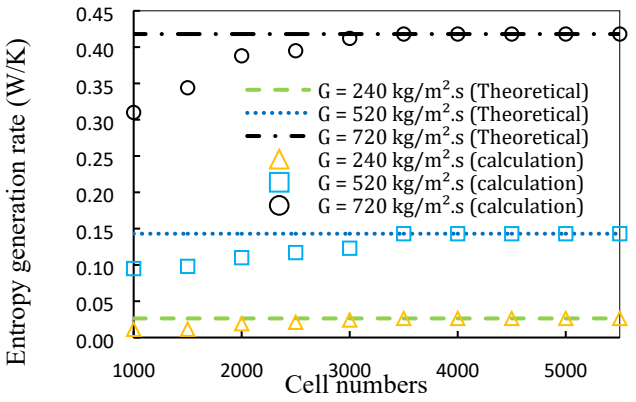

Fig. 3a: Grid independency and validation for helical coil simulation based on flow conditions in Table 2 and D_i = 8.3 mm and D_c = 305 mm.

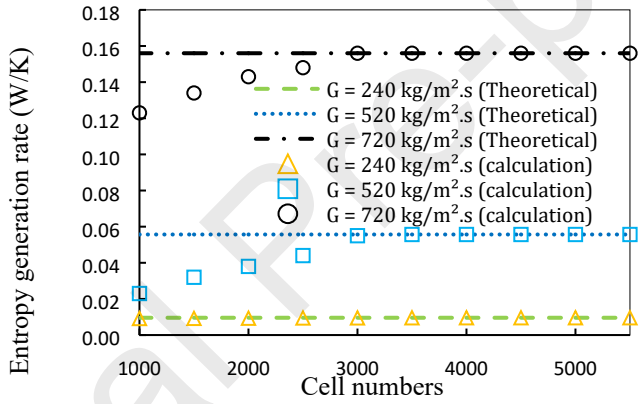

Fig. 3b: Grid independency and validation for straight tube simulation based on flow conditions in Table 2 and D_i = 8.3 mm.

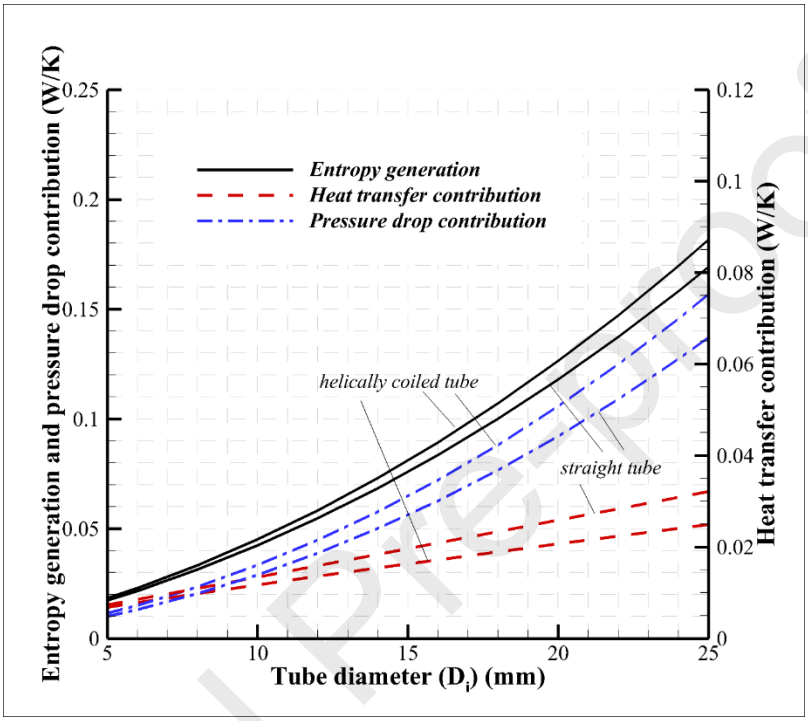

Fig. 4: Variation of total entropy generation and heat transfer and pressure drop contributions with tube diameter for flow conditions in Table 2 and a coil diameter of 305 mm.

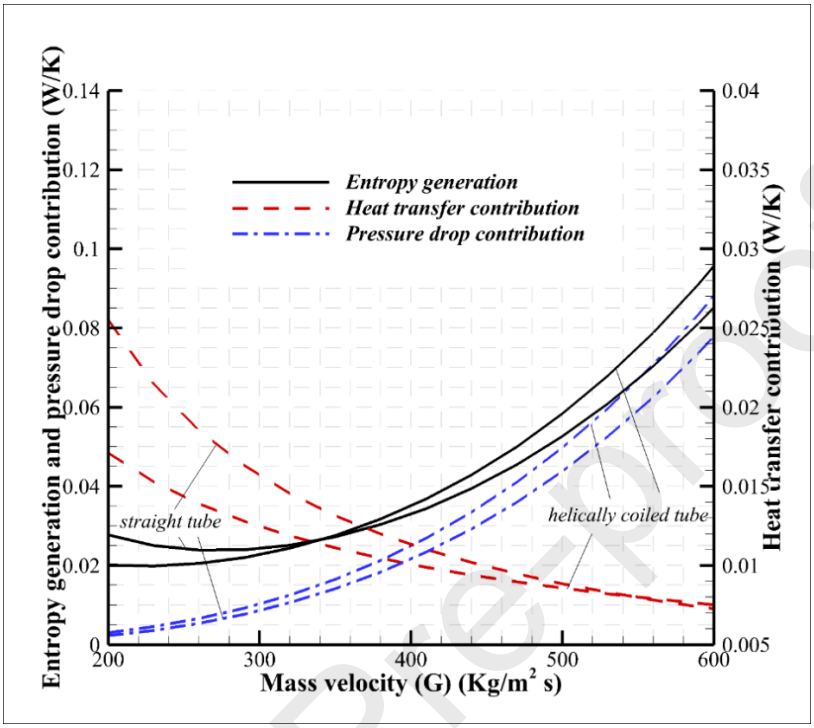

Fig. 5: Variation of total entropy generation and heat transfer and pressure drop contributions with mass velocity for flow conditions presented in Table 2 and tube and coil diameters of 8.3 mm and 305 mm, respectively.

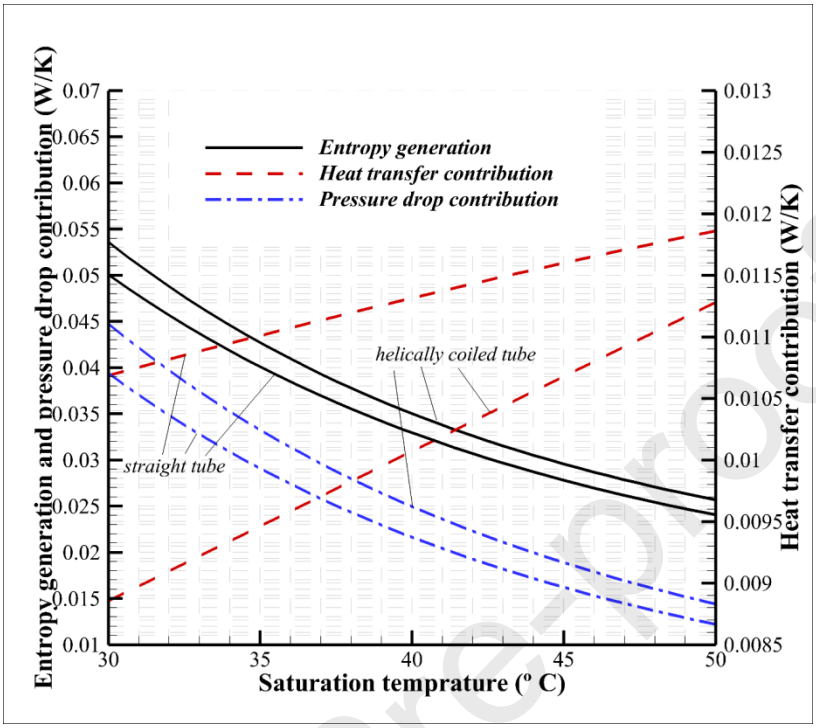

Fig. 6: Variation of total entropy generation and heat transfer and pressure drop contributions with saturation temperature for flow conditions in Table 2 and tube and coil diameters of 8.3 mm and 305 mm, respectively.

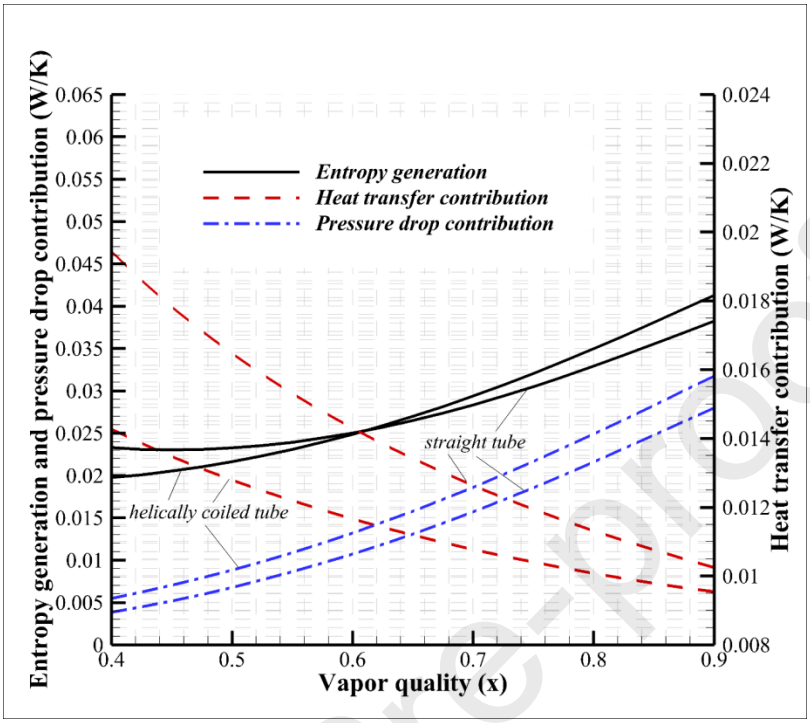

Fig. 7: Variation of total entropy generation and heat transfer and pressure drop contributions with vapor quality for flow conditions in Table 2 and tube and coil diameters of 8.3 mm and 305 mm, respectively.

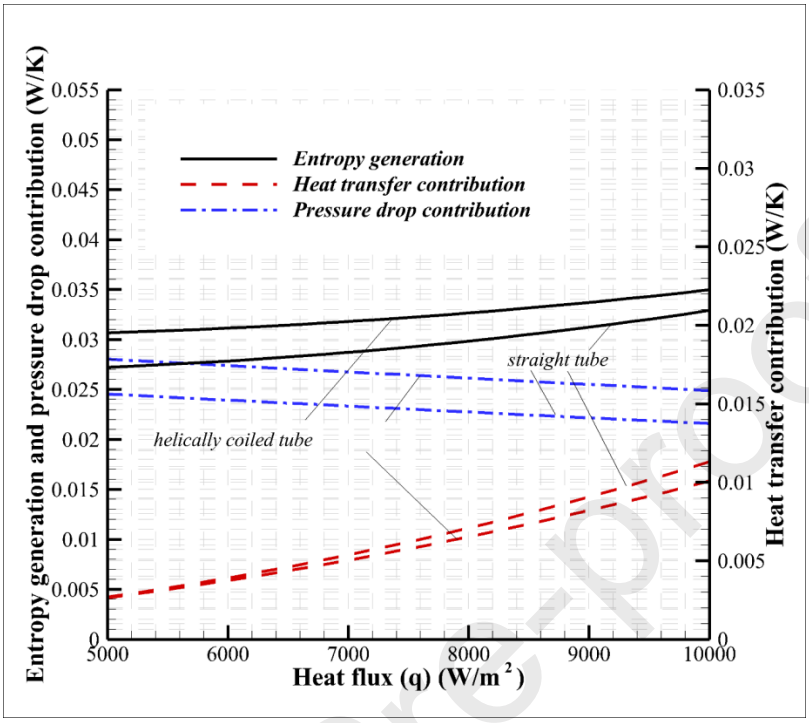

Fig. 8: Variation of total entropy generation and heat transfer and pressure drop contributions with wall heat flux for flow conditions in Table 2 and tube and coil diameters of 8.3 mm and 305 mm, respectively.

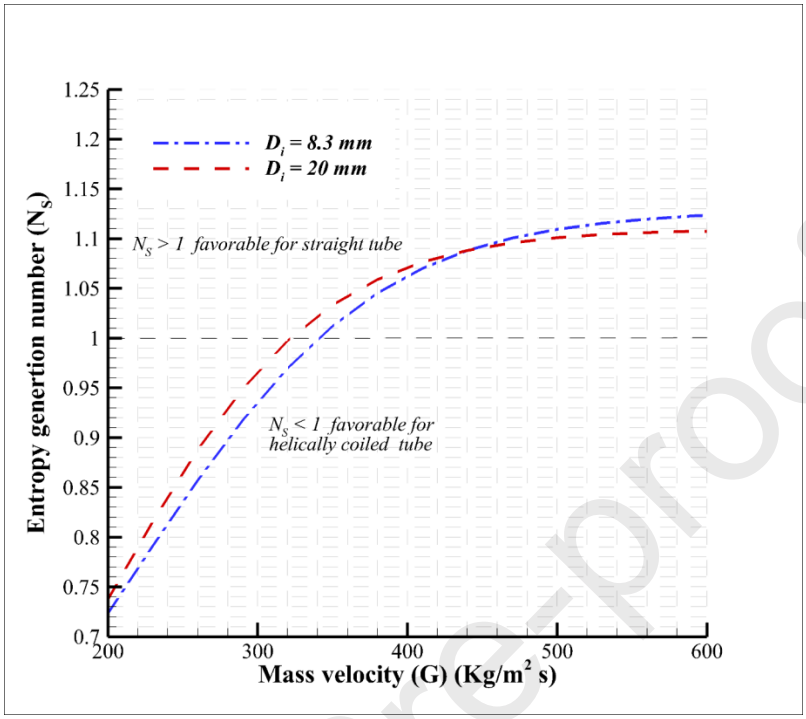

Fig. 9: Variation of N_s with mass velocity for two tube diameters (D_i = 8.3 mm and D_i = 20 mm), for D_c = 305 mm and flow conditions in Table 2.

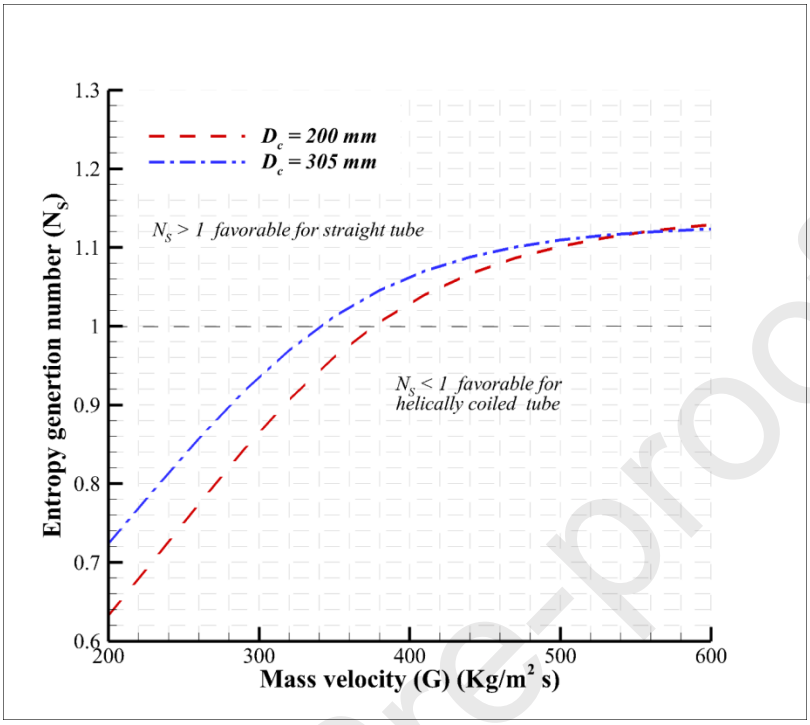

Fig. 10: Variation of N_s with mass velocity for two coil diameters (D_c = 200 mm and D_c = 305 mm), for D_i = 8.3 mm and flow conditions in Table 2.

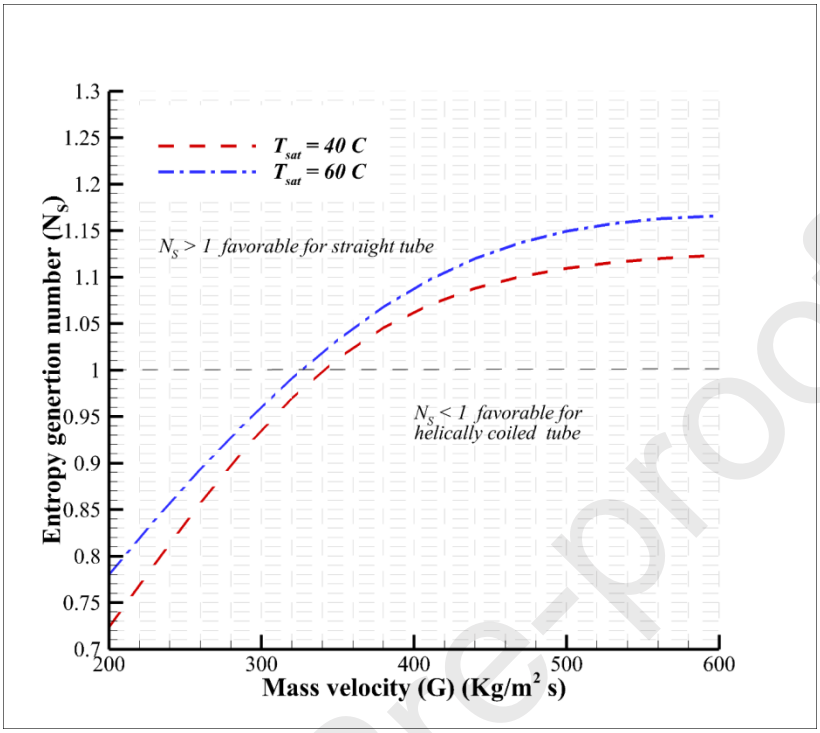

Fig. 11: Variation of N_S with mass velocity for two saturation temperatures (T_{sat} = 40 ℃ and T_{sat} = 60 ℃), for D_i = 8.3 mm, D_c = 305 mm, and other flow conditions in Table 2.

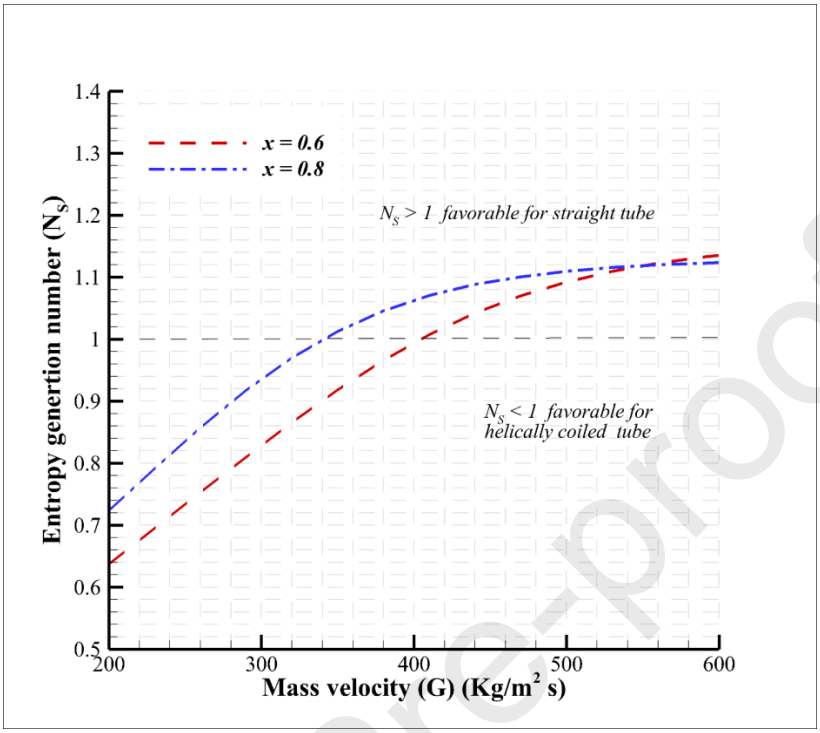

Fig. 12: Variation of N_s with mass velocity for two vapor qualities (x = 0.6 and x = 0.8), for D_i = 8.3 mm, D_c = 305 mm, and other flow conditions in Table 2.

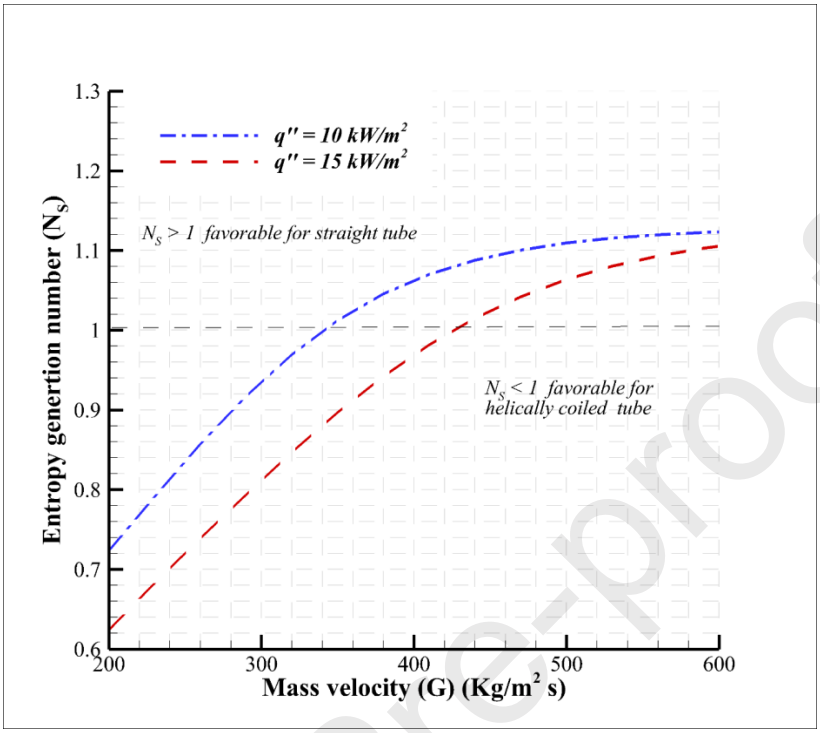

Fig. 13: Variation of N_S with mass velocity for two wall heat fluxes ($q'' = 10\ kW.m^{-2}$ and $q'' = 15\ kW.m^{-2}$), for $D_i = 8.3\ mm$, $D_c = 305\ mm$, and other flow conditions in Table 2.

1- Entropy generation of R134a flow condensation inside helical coils and straight tubes is studied and compared.
2- The impact of geometrical parameters on entropy generation is examined.
3- The impact of flow conditions on entropy generation is investigated.
4- Favorable geometrical and flow conditions at which the helical coils are of superior performance are determined